

DOI: 10.1002/adfm.200500293

Enhancement of Phosphorescence by Surface-Plasmon Resonances in Colloidal Metal Nanoparticles: The Role of Aggregates**

By Jacek C. Ostrowski, Alexander Mikhailovsky,* David A. Bussian, Melissa A. Summers, Steven K. Buratto, and Guillermo C. Bazan

The spectroscopic and near-field scanning optical microscopy (NSOM) studies of phosphorescent films doped with colloidal gold nanoparticles (NPs) are presented. Films with a high concentration of 2,3,7,8,12,13,17,18-octaethyl-21H,23H-porphine platinum(II) dispersed in a neutral polymer poly[(methyl methacrylate)-*co*-(ethyl acrylate)] demonstrate a twofold increase of the phosphorescence quantum yield after the addition of aggregated NPs. In materials doped with unaggregated particles, a decrease of the emission yield is observed. Theoretical modeling of the phosphorescence transients suggests a minimization of the triplet-triplet quenching owing to the presence of fast processes that decrease the concentration of chromophores in the excited state and may be both of radiative and non-radiative origin. NSOM examination of the films reveals increased light emission around large NP clusters. This observation demonstrates significant enhancement of the spontaneous emission rates by the large aggregates, although unaggregated NPs introduce mostly phosphorescence quenching sites.

1. Introduction

There has been strong interest in recent years in techniques enabling one to modify the rate of light emission by a chromophore. These methods, known as “radiative-decay engineering”,^[1] have been employed in biosensor applications,^[2] light-emitting diodes,^[3] and in the development of luminophores with improved performance.^[4] This technique relies on the increase of the spontaneous emission rate in emitters situated in the vicinity of metal structures where the density of photonic states is higher than in a homogeneous medium.^[5–7] The enhancement can be especially high if the optical transition frequency is resonant with the surface-plasmon (SP) oscillations in the metal. Increased rates of spontaneous emission can lead to enhancement of the chromophore’s emission quantum yield and significant reduction of the excited-state lifetime. SP-related enhancement of the emission rate has been observed on corrugated metal surfaces,^[8,9] noble-metal nanoparticles (NPs),^[10,11] and fractal-like structures.^[12]

Enhancement of the spontaneous emission rate is a near-field effect and is maximized in close proximity to the metal surface. Numerical modeling^[13,14] indicates that it decays significantly at distances from a NP’s surface comparable with the NP’s diameter. Besides the emission-rate acceleration, interactions with the metal surface may introduce non-radiative losses associated with Förster type energy transfer to the metal.^[1] The rate of this energy-transfer process generally scales as f/R^m , where f is the chromophore’s oscillator strength, R is the distance between the emitter and the metal surface, and m depends on geometric factors. For chromophores adjacent to subwavelength-sized metal NPs, the energy transfer has a $1/R^4$ dependence,^[15,16] unlike the $1/R^6$ dependence for adjacent point dipoles^[17] (for a two-dimensional metal surface one gets the well-known cubic dependence^[18]). A chromophore molecule placed in the vicinity of a metal particle experiences both emission-rate enhancement and quenching effects and the net balance of these phenomena is difficult to predict accurately in actual materials.

The introduction of a dielectric, optically transparent spacer between the NP surface and the chromophore can be used to minimize emission quenching by preventing the emitter from approaching the metal surface. At the same time, spatial separation between the chromophore and the metal may nullify the emission-rate-enhancement effect if both emission enhancement and quenching occur on the same length scale. Triplet emitters may have a significant advantage in this situation, because their oscillator strength is significantly smaller than those of singlet emitters and therefore the radius of efficient energy-transfer quenching is correspondingly smaller. The ratio of oscillator strengths for typical singlet and triplet emitters can be estimated as a ratio of their radiative lifetimes. Considering values of 1 ns and 10 μ s, the ratio of the transition moments can be estimated to be of the order of 10 000. Since the energy-

[*] Dr. A. Mikhailovsky, Dr. J. C. Ostrowski, D. A. Bussian, Dr. M. A. Summers, Prof. S. K. Buratto, Prof. G. C. Bazan
Department of Chemistry and Biochemistry, University of California
Santa Barbara, CA 93106-9510 (USA)
E-mail: mikhailovsky@chem.ucsb.edu
Prof. G. C. Bazan
Institute for Polymers and Organic Solids, University of California
Santa Barbara, CA 93106-9510 (USA)

[**] The authors thank the Office of Naval Research (grant number N-00014-04-0411) and the Department of Energy (grant number DE-FC26-04NT42277) for funding of the research. The authors also thank Richard Puestow, Stefan Kämmer and Veeco Metrology group for providing Aurora 3 NSOM and UV-enhanced NSOM tips, as well as for their helpful assistance.

transfer quenching rate scales as f/R^4 (as in metal NPs^[15]), one can estimate that for triplet emitters similar levels of emission-quenching efficiency are achieved at distances from the metal surface ten times smaller than for singlet chromophores. For instance, the effective quenching distance for fluorescein molecules in the vicinity of 20 nm gold NPs has been measured to be approximately 20 nm.^[15] From these data, we can estimate that triplet emitters more than 2 nm away from the NP surface will experience less quenching, while at the same time emission-rate enhancement will take place because the spatial distribution of the density of photonic states does not depend on f . The total net effect (enhancement minus quenching) would result in an emission increase. Under these circumstances, thin spacers, such as a layer of organic molecules or an inorganic dielectric shell, may be considered to minimize the non-radiative losses in SP-enhanced phosphorescent materials.

The use of colloidal, noble-metal NPs for radiative-decay engineering in thin-film materials has several advantages in comparison with using other plasmonic structures (e.g., periodically modulated or randomly corrugated metal surfaces^[9]). Indeed, the SP resonance in silver and gold NPs is situated in the visible range of the spectrum; its wavelength can be controlled through NP size and shape variation to match the chromophore's emission frequency.^[19,20] Also, these NPs can be synthesized in sizeable quantities using well-established chemical techniques and their surface can be functionalized easily to suit specific application requirements.

2. Results and Discussion

We have chosen to investigate the possibility of increasing the radiative decay in thin films containing 2,3,7,8,12,13,17,18-octaethyl-21*H*,23*H*-porphine platinum(II) (PtOEP), an emitter used in the fabrication of phosphorescent organic light-emitting diodes (PhOLEDs). The performance of these devices is often limited by either saturation of the chromophore or by multiparticle recombination processes, such as triplet-triplet annihilation (TTA)^[21] and triplet-polaron annihilation,^[22] due to the very low rate of the light emission ($\tau_{\text{Rad}} \sim 90 \mu\text{s}$). In this contribution, we focus on ways by which NPs can influence the optical performance of PhOLEDs through variation of the emission rates and control over multiparticle annihilation processes. These experiments were performed using optical excitation of the phosphorescence in a non-conductive matrix, because, for incorporation of NPs into functioning devices, a better understanding of how they affect processes such as charge injection, charge transport, and film morphology is required.

In this paper, we demonstrate that in blends of a neutral polymer, poly[(methyl methacrylate)-*co*-(ethyl acrylate)] (5%) with PtOEP, the phosphorescence yield increases after addition of aggregated gold NPs coated with an organic layer. This protective shell is expected to decrease phosphorescence quenching and ensure solubility of the NPs in nonpolar organic solvents. Doping with gold NPs leads to a significant reduction

of non-radiative losses caused by the TTA in blends with a high PtOEP concentration. A correlation is made between phosphorescence-lifetime data and the emission quantum yields, which suggests that the SP enhancement of emissive processes is observed in samples with aggregated NPs where the SP enhancement spectrum has a better overlap with the PtOEP emission band. In samples with unaggregated NPs the SP enhancement is masked by NP-induced non-radiative processes. Near-field scanning optical microscopy (NSOM)^[23] was used to elucidate enhancement regions surrounding the NPs.

Our studies utilized NPs with average radii of ca. 7 nm overcoated with dodecanethiol molecules. A layer of molecules was attached to the NP's surface through thiol groups. The extended alkyl chains provided solubility in organic non-polar solvents and served as a protective layer to reduce the energy-transfer-induced quenching (estimated thickness of the organic cap is 2–3 nm). Also, we used tetraoctylammonium bromide (TOABr) in several batches of the NPs to manipulate the size distribution of the NPs. It is known that TOABr can induce NP aggregation by alkyl-chain interdigitation,^[24] which ultimately shifts the plasmon resonance to lower energies. Several batches of NPs were synthesized using a modified Perry reaction,^[25] which is TOABr-free (AuNPs) and allows one to obtain unaggregated NPs. Figure 1 shows the absorption spectra of the two samples of particles synthe-

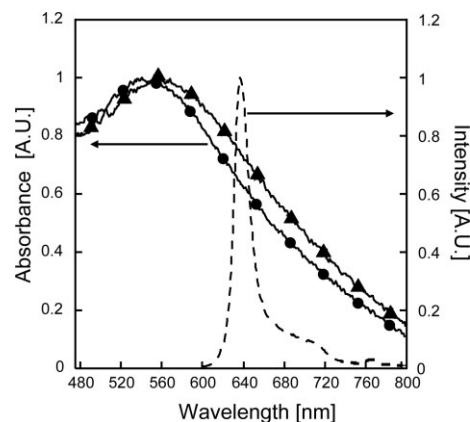


Figure 1. Absorbance of NPs synthesized with tetraoctylammonium bromide, Au_{TOABr}NPs (solid triangles). Absorbance of gold NPs synthesized without tetraoctylammonium bromide, AuNPs (solid circles). The emission of PtOEP (dashed curve) is also shown.

sized and the emission spectrum of the PtOEP chromophore. Particles made using TOABr (Au_{TOABr}NPs) have a broader and red-shifted plasmon band, compared to AuNPs; this is consistent with aggregation.^[26] PtOEP-PMMA (PMMA: poly(methyl methacrylate)) film samples were prepared by blending the chromophore, metal NPs, and polymer host (PMMA) with a solvent. The blend was cast on a pre-cleaned glass or quartz substrate. The concentration of the NPs in the film and its thickness were estimated using UV-vis absorption spectroscopy and from the mass of the metal added to the

blend. Film-thickness measurements were performed using a profilometer and an atomic force microscope (AFM).

Table 1 shows the concentration of NPs in different films, as well as the average interparticle separation, assuming a random spatial distribution of NPs, and the fractional volume of the

Table 1. Average distance between the particles and volume taken up by the non-aggregated gold NPs.

Number of particles per cubic micrometer	Distance between surfaces [nm]	Volume of gold particles taken up in the matrix [%]
3870	6.7	6.9
7250	4.1	13
12810	2.2	23

film occupied by the metal. The latter values were obtained from the weight ratios of the polymer to the gold NPs. Even in the blends with the highest content of gold NPs, the relative volume of the sample taken by the NPs does not exceed 23%. Thus, the majority of the volume in the films is the PMMA host matrix doped with the PtOEP triplet emitter. However, aggregation of NPs may lead to an increased average distance between the surfaces of the metal clusters compared to that illustrated for a homogeneous distribution of the NPs. Clusters of NPs will be more prevalent using Au_{TOABr}NPs relative to AuNPs. In this case, additional enhancement of the emission rate may be observed as a side effect of the cluster formation owing to an increase of the effective particles' size and field-amplification phenomena in fractal-like structures and rough surfaces.^[27]

Figure 2 shows the phosphorescence quantum yield determined by the use of an integrating sphere against the NP concentration. The emission quantum yield reveals different trends in films containing Au_{TOABr}NPs or AuNPs. In samples doped with AuNPs the quantum yield decreases slightly as the NP concentration increases. In contrast, samples with Au_{TOABr}NPs demonstrate almost a twofold increase of the emission, compared to the undoped samples. Use of colloidal gold NPs allowed us to exclude from consideration effects associated with

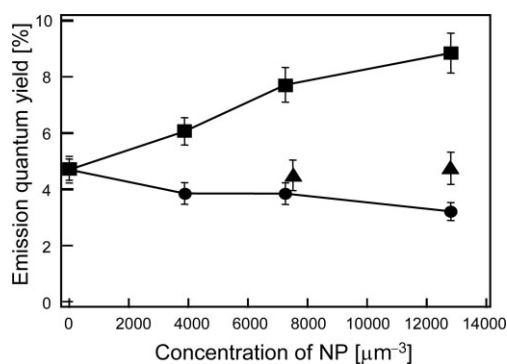


Figure 2. Phosphorescence quantum yield of PtOEP-PMMA films (16 wt%) as a function of NP concentration. Au_{TOABr}NPs (squares), AuNPs (circles), silica spheres (triangles).

an effective increase of the absorption cross section of the chromophore due to local field enhancement by the metal surface. Our chromophore was excited either at 363 or 354 nm, which is far away from the SP band in gold NPs (ca. 540 nm).

A set of control experiments was undertaken to exclude waveguiding-related effects and phenomena attributed to the decreased density of the chromophore (relative to films without NPs). We prepared PtOEP-PMMA samples containing silica nanospheres with a mean diameter of approximately 80 nm and displaced the same volume of matrix and chromophore as in the experiments with gold NPs. As shown in Figure 2, control samples showed no dependence of the emission yield on silica-nanosphere concentration or perturbations on the PtOEP emission lifetime (not shown). This observation was anticipated since the addition of metal NPs should not influence significantly the mean distance between PtOEP molecules, which are much smaller than NPs.

Despite the phosphorescence quantum-yield behavior being consistent with the SP enhanced-emission model, the emission transients exhibited what at first sight appears to be an opposite trend. Figure 3 shows that after addition of metal NPs the decay of the phosphorescence became apparently slower and was non-exponential. Interestingly, similar changes of the phos-

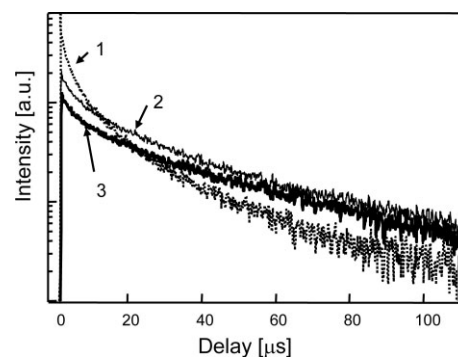


Figure 3. Phosphorescence decay transients in PtOEP-PMMA films as a function of Au_{TOABr}NP concentration. No NPs (1), 768 μm⁻³ (2), 12 800 μm⁻³ (3). Samples with AuNPs exhibit similar behavior.

phorescence decay were observed in samples doped with Au_{TOABr}NPs and AuNPs. To explain this phenomenon, we performed a detailed analysis of the energy-relaxation dynamics in our samples. In particular, we considered a multiexciton non-radiative recombination process, such as TTA.

The rate equation describing the evolution of the density of excited states can be written as^[28]

$$\dot{N} = -(k_R + k_{NR})N - \beta \frac{N^2}{t^z} \quad (1)$$

where N is the density of the excited states, k_R and k_{NR} are the chromophore's intrinsic radiative and non-radiative recombination rates, respectively, β is the TTA rate constant, t is time, and z describes the exciton wandering dimensionality, where $z = 0$ corresponds to 3D wandering and $z = 1$ describes the situ-

ation of completely immobilized exciton (no wandering). Equation 1 can be solved analytically and an expression for the time-dependent phosphorescence intensity $I(t)$ can be obtained by taking into account that $I(t) = k_R N(t)$:

$$I(t) = \frac{k_R e^{-t/\tau} N_0}{t^z + N_0 \beta \tau t^z \Gamma(1-z) - N_0 \beta \tau^{z-1} t^z \Gamma(1-z, t/\tau)} \quad (2)$$

In this expression, N_0 is the density of excited states at $t=0$, τ is the intrinsic emission decay time constant, including both radiative and non-radiative mechanisms ($\tau = 1/(k_R + k_{NR})$), $\Gamma(x)$ is the Euler gamma function, and $\Gamma(a,x)$ is the incomplete gamma function. When $\beta=0$ (no TTA) Equation 2 reduces to the well-known exponential expression for emission decay.

Figure 4A shows that optimization of N_0 , β , τ , and z yields adequate modeling of the measured decay profiles with excep-

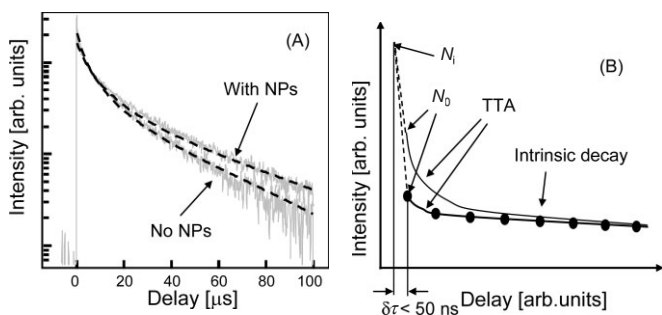


Figure 4. A) Fitting of the phosphorescence decays (normalized) using the TTA model. B) Scheme illustrating suppression of TTA by a fast excited state depopulation in NP-doped samples.

tion of a very short delay time comparable with the width of the instrument response function (ca. 50 ns). The results of the data analysis for samples prepared with Au_{TOABr}-NPs and AuNPs are summarized in Table 2. The parameters β , τ , and z are nearly identical for samples with the same PtOEP concentration. The exciton wandering parameter z is close to 0, indi-

Table 2. Phosphorescence-emission yield and fitting parameters for the TTA mathematical model. (Units for β and N_0 are not shown, since the population density was not determined in absolute units.)

Gold NPs concentration, [μm^{-3}]	Emission quantum yield [%]	Intrinsic emission lifetime, τ [μs]	TTA constant, β	Exciton migration parameter, z	N_0
16 % PtOEP with AuNPs					
0	4.5	26.9	1.18	0.0025	0.22
3870	3.9	24.5	1.18	0.007	0.15
7250	3.9	22.6	1.20	0.007	0.13
12810	3.6	22.5	1.18	0.009	0.10
16 % PtOEP with Au _{TOABr} -NPs					
0	4.5	26.7	1.18	0.009	0.11
3870	5.9	26.4	1.18	0.008	0.10
7250	7.7	26.2	1.18	0.008	0.08
12810	8.5	25.7	1.17	0.004	0.03

cating unrestricted 3D wandering of excitons in the film. There is no significant variation in the values of the intrinsic excited-state decay time τ when the same PtOEP concentration is used. However, the initial amplitude of the excited-state density, N_0 , decreases considerably as the NP load in the film increases. A decrease of N_0 explains the apparent slowing down of the emission rate. Indeed, fast multiexciton annihilation becomes less pronounced because it is proportional to the square of the excitations density (Fig. 4B). In our case, N_0 can change due to different phenomena. First, a different number of excited states can be generated by the laser pulse. However, the optical density of the NP-doped films at the excitation wavelength is small and absorption of NPs cannot account for the large variations of N_0 . Second, variation of N_0 can be attributed to the presence of an initial fast component of the decay that can not be resolved by our experimental setup, which has a temporal resolution of about 50 ns. In this case, the actual number of excited states generated by the pump pulse is identical in all samples (N_i in Fig. 4B). However, it decreases rapidly to the value N_0 which is sample specific and can be modulated by variation of the NPs load. This decay component is not accounted for in our modeling and parameter N_0 can be treated in our case as a density of excited states at some small delay after the laser pulse $\delta t \sim 50$ ns. The presence of this fast-decay component in NP-doped films leads to the situation where a significant amount of triplet excitons may decay to the ground state rapidly thus reducing the efficiency of TTA. We propose that the fast drop of the excitation density and associated reduction of TTA is due to an accelerated emission rate and/or a quenching by metal NPs in a certain fraction of the chromophore species (Fig. 4B). The amplitude and the time constant of this fast component depend on the concentration of metal NPs in the sample. Efforts have been directed to detect and characterize the initial fast component of the emission decay using a time-correlated single-photon counting setup. The measurements indicate the presence of the phosphorescence decay component that has a sub-50 ns lifetime. However, these data can not be characterized quantitatively, because the long radiative lifetime in PtOEP leads to distortions of the emission transients caused by photon-count pile-up effects.

Examination of Table 2 shows that there is no increase of the phosphorescence yield in films containing AuNPs, although decreased signatures of TTA in the emission transients indicate the presence of the fast-decay component. In contrast, films prepared with Au_{TOABr}-NPs demonstrate significant enhancement of the emission efficiency. Using these considerations, and comparing emission-yield behavior as a function of the particle concentration, we conclude that in samples with aggregated Au_{TOABr}-NPs we observe the enhancement of radiative recombination, while in samples with non-aggregated AuNPs, the situation is the opposite and addition of NPs introduces fast quenching processes. This can be explained by the presence of large aggregates of NPs in Au_{TOABr}-NP samples. They can affect the rate of light emission in several ways. First, they have better overlap of the surface-plasmon resonance and PtOEP emission bands. Indeed, in non-aggregated particles the shift between the SPR band (maximum at ~ 530 nm) and the PtOEP

emission wavelength (646 nm) is large, and SPR-assisted emission is quite inefficient. Second, the aggregation could be considered as an effective increase of NP size, thus leading to increased local fields and emission rates. Finally, randomly assembled clusters of NPs can generate field “hot spots”,^[12] providing very large local fields. Also, in small gold NPs, the SP has mostly absorptive character,^[29] leading to significant energy losses in the chromophore. In contrast, in large NPs, the dominant mechanism of the SP's interaction with light is the lossless scattering. The presence of large aggregates in Au_{TOABr}-NPs is confirmed by a red-shift of the SPR maximum ($\Delta\lambda = 32$ nm) and broadening of the SPR peak that can be seen in Figure 1. If one considers TOABr-induced aggregation as a formation of spherical NPs with larger diameter, the shift of the SPR bands shown in Figure 1 corresponds to an increase of the effective diameter of NPs from 7 to ca. 80 nm. Figure 5 demonstrates the spectra of averaged local field enhancement,

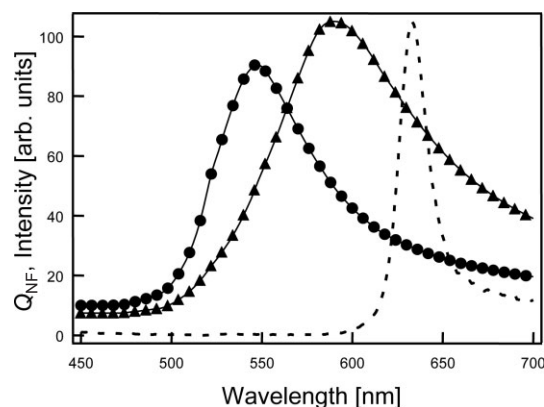


Figure 5. Calculated average local field enhancement (Q_{NF}) at the surface of gold NPs with a diameter of 7 nm (circles) and 80 nm (triangles) in PMMA (refractive index, $n=1.49$). PtOEP phosphorescence spectrum (dashed line).

calculated using an apparatus outlined in the literature^[29] for spherical NPs with diameters of 7 and 80 nm, along with the PtOEP phosphorescence spectrum. As one can see, large particles provide significant field amplification and an increase of the emission rate at PtOEP emission wavelengths.

To visualize the enhancement of the emission processes on a microscopic level and estimate the extent of the enhancement region, films were characterized using NSOM. This technique enables one to perform simultaneous topographic and near-field optical characterization of surfaces. The aperture (ca. 50 nm) of the fiber-optic probes used in this technique determines the optical resolution, enabling sub-diffraction-limited luminescence imaging. NSOM data for a PtOEP-PMMA film (with no gold NPs) reveal a uniform, featureless film (not shown). The emission intensity of 100 counts per second for this sample is significantly lower than the lowest intensities observed in the films containing Au_{TOABr}-NPs. Generally, the emission throughout films containing Au_{TOABr}-NPs is consistently brighter relative to a PtOEP-PMMA blend film using similar excitation parameters. Figure 6 shows the topography

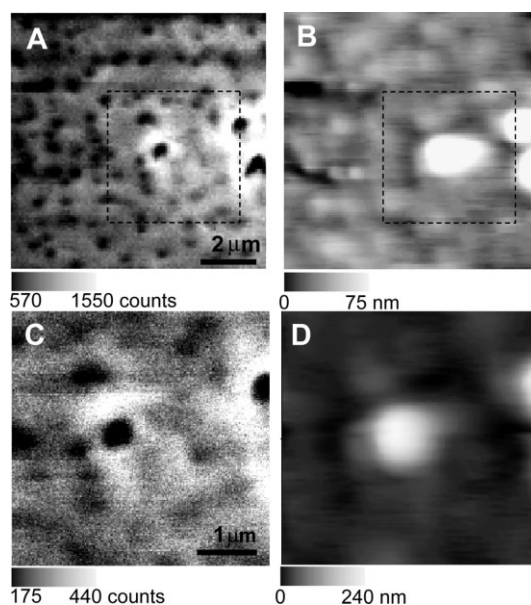


Figure 6. NSOM images of PtOEP-PMMA films doped with Au_{TOABr}-NPs. 10 $\mu\text{m} \times 10 \mu\text{m}$ scan of emission intensity (A) at 646 nm, and topography (B). C,D) Corresponding images of the 4.3 $\mu\text{m} \times 4.3 \mu\text{m}$ -boxed region in images (A) and (B).

and corresponding emission images of a Au_{TOABr}-NP-PtOEP blend film (16 wt % PtOEP in PMMA matrix, ca. 1.2×10^5 particles per cubic micrometer), revealing gold NP aggregation on length scales ranging from tens to hundreds of nanometers. The dark features in the emission (Fig. 6A,C) correspond to the positions of gold NP aggregates in the film, which are expected to be non-emissive and opaque at the excitation wavelength (363 nm line of an Ar-ion laser). NP aggregates are more easily observed in the emission images than in the topography images. This is particularly true for the smaller (≤ 50 nm) aggregates where many of the particles are embedded below the film surface. The large clusters on the right-hand side of the topography trace in Figure 6B are approximately 200 nm in diameter, from the topographic images. However, owing to their large diameter, NSOM tips are not reliable for measuring lateral dimensions of surface features,^[30] only the height is determined correctly for topographic features.

The largest gold NP clusters are surrounded by the brightest PtOEP phosphorescence in the emission images. Nanoscale emission spectra obtained in these bright regions are identical to the bulk emission. Using topography measurements in numerous scans, we observed an average NP aggregate diameter of ca. 70 nm. Because the luminescence intensity is relatively high throughout the film, we conclude that we see enhancement from a range of nanocluster sizes, but the largest clusters yield the largest enhancements.

One should be careful analyzing the emission patterns obtained using the NSOM technique. Artifacts introduced by the metal-coated NSOM fiber-optic tip can distort the emission intensity surrounding tall topographic features.^[31] These artifacts generally lead to an anisotropic decrease in luminescence intensity appearing as a shadow near the feature due to the tip

lifting off the sample as it scans the feature. In contrast, we observe nearly a two-fold increase in luminescence intensity surrounding the largest topographic features that extend up to several tip diameters. At this distance, tip artifacts should not distort the detected luminescence. From the NSOM scans, we observed that the extent of the enhanced emission regions around the large clusters is comparable with their linear dimensions. This conclusion is in agreement with theoretical calculations.^[13] Unfortunately, the poor topographic and optical resolution of NSOM (compared to NP size) does not allow quantitative measurements of the phosphorescence enhancement, and correlation between the NPs morphology and the phosphorescence enhancement was performed only qualitatively.

The NSOM data are in good agreement with our interpretation of results obtained in macroscopic-scale studies. Indeed, one would expect to observe larger enhancement of the phosphorescence in larger NPs and rough aggregates.^[4,32] The latter phenomenon could be surprisingly efficient since local roughness in such clusters can generate extremely high local fields.^[12,32] The presence of such aggregates and NPs can be seen from Figure 1 and was discussed previously. It is worth mentioning that the average diameter of aggregates determined from the *z*-coordinate NSOM measurements is similar to the effective diameter of NPs determined from the optical-extinction spectra (70 and 80 nm, respectively).

3. Conclusions

An enhancement of emission and a decrease in triplet–triplet quenching was observed upon the introduction of gold NPs into a polymer film containing PtOEP. An observed twofold increase of the emission efficiency was attained at the highest NP concentrations with an aggregation-promoting agent. Modeling of the phosphorescence transients and NSOM studies indicates a fast component of the emission decay, which is introduced to chromophores surrounding aggregated NPs. At the same time, non-aggregated NPs do not enhance emissive properties of the triplet emitter due to poor overlap of the SPR enhancement and phosphorescence bands and an increased emission quenching. Nevertheless, they suppress TTA by decreasing the density of excitations through non-radiative processes. Simple materials blending technology used for the fabrication of samples can be extended easily to the preparation of PhOLEDs with enhanced efficiency and to devices which are less prone to multi-exciton annihilation processes.

4. Experimental

All chemicals were purchased from Aldrich and used as obtained. Gold NPs containing TOABr (average radius of 7 nm) [33], gold NPs without TOABr [25] and silica spheres [34,35] capped with a methacrylate group [36] were prepared by using literature procedures. Solutions for casting polymer/phosphor films were prepared by mixing stock solutions of 1.5% Au_{TOABr}NPs, 3% AuNPs, 1.5% PtOEP, and 4% PMMA in CH₂Cl₂. Quantum yields of the phosphorescence were mea-

sured according to a literature procedure [37]. For our measurements we used an Ar-ion laser (Spectraphysics Beamlok 2060) emitting at 363 nm to excite the sample. Quantum-efficiency measurements used a 6 inch (1 inch = 0.0254 m) BaSO₄-coated integrating sphere (Lab-Sphere).

Emission-lifetime measurements were carried out inside an evacuated cryostat using a homemade single-shot emission-lifetime-measurement spectrometer. Measurements were performed at room temperature and an evacuated cryostat was used solely to avoid photooxidation effects. A Nd:YAG laser output upconverted to 355 nm through the third harmonic generation process was used as the excitation beam. Excitation occurred at a 45° angle relative to the detector. The phosphorescence was collected by an optical system and dispersed using an Acton Research SP-500 spectrometer. A Hamamatsu R-928 photomultiplier tube (PMT) was used as a detector and was connected directly to the input of a digital oscilloscope (Lecroy 9200) which digitized the transients of the PMT's current and was triggered by the laser Q-switch gating signal. Background signals caused by the PMT's dark current and electrical noise were also collected and subtracted from the sample signal. Several measurements were performed on a similar setup using the second harmonic of the Ti:sapphire laser (ca. 380 nm, ca. 100 fs pulse duration) as the excitation light. In all cases, the repetition rate of the laser was low enough to ensure complete disappearance of the phosphorescence between two laser pulses. The temporal resolution of the setup, ca. 50 ns, was determined by measurements of the excitation pulse scattering and limited by the detector response time.

Transmission electron microscopy imaging of the nanoparticles was carried out using a JOEL 2010HR instrument. Film thickness was evaluated using an AFM and all films were in the range of 50–75 nm thick. In such thin films, light-waveguiding effects are negligible and do not affect emission-yield measurements. NSOM data were acquired using a commercially available NSOM apparatus (Aurora-3, Veeco Metrology). The microscope uses a tuning-fork shear-force feedback mechanism to maintain a constant sample–probe distance of ca. 7 nm. Samples were excited with the 363 nm line of an Ar-ion laser (Beamlock 2060, Spectraphysics) coupled to aluminum-coated UV-enhanced fiber probes (1640-UV, Veeco Metrology) with ca. 50 nm apertures. All optical fibers were multimode with enhanced UV transmission (Thorlabs). Luminescence was collected in the transmission geometry. The optical-detection pathway consisted of a series of optical filters (Schott Glass, Newport; Interference filters, Chroma) as needed and a non-polarizing 50/50 beamsplitter. The beamsplitter directed emission to the active area of a Si avalanche photodiode (SPCM-14, Perkin–Elmer) and into a monochromator (SP 300i, Acton Research) coupled to a liquid-nitrogen-cooled charge-coupled device camera (Spec-10, Princeton Instruments).

Received: May 13, 2005

Final version: October 18, 2005

Published online: May 4, 2006

- [1] J. R. Lakowicz, *Anal. Biochem.* **2001**, 298, 1.
- [2] J. R. Lakowicz, *Anal. Biochem.* **2005**, 337, 171.
- [3] K. Okamoto, I. Niki, A. Shvartser, Y. Narukawa, T. Mukai, A. Scherer, *Nat. Mater.* **2004**, 3, 601.
- [4] S. L. Pan, L. J. Rothberg, *J. Am. Chem. Soc.* **2005**, 127, 6087.
- [5] W. L. Barnes, *J. Mod. Opt.* **1998**, 45, 661.
- [6] M. Woldeyohannes, S. John, *Phys. Rev. A* **1999**, 60, 5046.
- [7] P. T. Worthing, W. L. Barnes, *J. Opt. A* **1999**, 1, 501.
- [8] A. Weissberger, *Physical Methods of Chemistry*, Vol. 3, Wiley, New York **1972**.
- [9] H. Raether, *Surface Plasmons on Smooth and Rough Surfaces and on Gratings*, Vol. 111, Springer, Berlin, **1988**.
- [10] O. Kulakovich, N. Strekal, A. Yaroshevich, S. Maskevich, S. Gaponenko, I. Nabiev, U. Woggon, M. Artemyev, *Nano Lett.* **2002**, 2, 1449.
- [11] K. T. Shimizu, W. K. Woo, B. R. Fisher, H. J. Eisler, M. G. Bawendi, *Phys. Rev. Lett.* **2002**, 89, 117401.

- [12] V. P. Drachev, W. T. Kim, V. P. Safonov, V. A. Podolskiy, N. S. Zakovryashin, E. N. Khaliullin, V. M. Shalaev, R. L. Armstrong, *J. Mod. Opt.* **2002**, *49*, 645.
- [13] H. Chew, *J. Chem. Phys.* **1987**, *87*, 1355.
- [14] D. A. Weitz, S. Garoff, J. I. Gersten, A. Nitzan, *J. Chem. Phys.* **1983**, *78*, 5324.
- [15] C. S. Yun, A. Javier, T. Jennings, M. Fisher, S. Hira, S. Peterson, B. Hopkins, N. O. Reich, G. F. Strouse, *J. Am. Chem. Soc.* **2005**, *127*, 3115.
- [16] I. A. Larkin, M. I. Stockman, M. Achermann, V. I. Klimov, *Phys. Rev. B* **2004**, *69*, 121403.
- [17] T. Forster, *Ann. Phys.* **1948**, *2*, 55.
- [18] H. Morawitz, *Phys. Rev.* **1969**, *187*, 1792.
- [19] P. C. Andersen, K. L. Rowlen, *Appl. Spectrosc.* **2002**, *56*, 124.
- [20] K. L. Kelly, E. Coronado, L. L. Zhao, G. C. Schatz, *J. Phys. Chem. B* **2003**, *107*, 668.
- [21] M. A. Baldo, C. Adachi, S. R. Forrest, *Phys. Rev. B* **2000**, *62*, 10967.
- [22] F. C. Chen, Y. Yang, M. E. Thompson, J. Kido, *Appl. Spectrosc.* **2002**, *80*, 2308.
- [23] G. M. Credo, D. L. Winn, S. K. Buratto, *Chem. Mater.* **2001**, *13*, 1258.
- [24] A. Badia, L. Cuccia, L. Demers, F. Morin, R. B. Lennox, *J. Am. Chem. Soc.* **1997**, *119*, 2682.
- [25] W. Wenseleers, F. Stellacci, T. Meyer-Friedrichsen, T. Mangel, C. A. Bauer, S. J. K. Pond, S. R. Marder, J. W. Perry, *J. Phys. Chem. B* **2002**, *106*, 6853.
- [26] J. J. Storhoff, A. A. Lazarides, R. C. Mucic, C. A. Mirkin, R. L. Letsinger, G. C. Schatz, *J. Am. Chem. Soc.* **2000**, *122*, 4640.
- [27] V. M. Shalaev, R. Botet, A. V. Butenko, *Phys. Rev. B* **1993**, *48*, 6662.
- [28] S. A. Bagnich, A. V. Konash, *Chem. Phys.* **2001**, *263*, 101.
- [29] B. J. Messinger, K. U. Vonraben, R. K. Chang, P. W. Barber, *Phys. Rev. B* **1981**, *24*, 649.
- [30] K. D. Weston, J. A. DeAro, S. K. Buratto, *Rev. Sci. Instrum.* **1996**, *67*, 2924.
- [31] G. A. Valaskovic, M. Holton, G. H. Morrison, *J. Microsc.* **1995**, *179*, 29.
- [32] B. Nikoobakht, M. A. El-Sayed, *J. Phys. Chem. A* **2003**, *107*, 3372.
- [33] M. Brust, J. Fink, D. Bethell, D. J. Schiffrin, C. Kiely, *J. Chem. Soc. Chem. Commun.* **1995**, 1655.
- [34] A. P. Philipse, A. Vrij, *J. Colloid Interface Sci.* **1989**, *128*, 121.
- [35] W. Stober, A. Fink, E. Bohn, *J. Colloid Interface Sci.* **1968**, *26*, 62.
- [36] L. M. Liz-Marzán, M. Giersig, P. Mulvaney, *Langmuir* **1996**, *12*, 4329.
- [37] N. C. Greenham, I. D. W. Samuel, G. R. Hayes, R. T. Phillips, Y. Kessener, S. C. Moratti, A. B. Holmes, R. H. Friend, *Chem. Phys. Lett.* **1995**, *241*, 89.